

Restricted Gas Diffusion in a Unique Porous Medium—Human Lung

Jason C. Woods,^{1,2} Dimitriy A. Yablonskiy,^{1,2} Mark S. Conradi^{2,1}

¹ Department of Radiology, Washington University, St. Louis, Missouri, USA

² Department of Physics, Washington University, St. Louis, Missouri, USA

Corresponding author:

Jason C. Woods

Washington University

One Brookings Drive, CB 8131

St. Louis, MO 63110

314-935-6220 (office)

314-935-6219 (fax)

E-Mail: jason.woods@wustl.edu

Abstract

Restricted diffusion of gas in the lung is in many ways similar to restricted diffusion in other porous media: atomic collisions with boundaries restrict the measured value, and there is a critical dependence on the time and distance scales of the measurement. The large free diffusivity of gases allows large pores (300 microns or larger) to be studied. The high signals of hyperpolarization permit rapid diffusion imaging of the gas itself, though fluorinated hydrocarbons are simple by comparison and are a potential alternative. The complicated nature of bifurcating human lung structure provides challenges in interpretation of results of restricted diffusion. At times sufficiently short, the short-time slope of $D(t)/D_0$ can be related to the surface-to-volume ratio - an important measure of lung structure and early emphysema. During times of a few milliseconds, diffusion anisotropy is observed, and the principal components of diffusion are related to geometric parameters of individual airways within the pulmonary acinus. This permits regional *in-vivo* lung morphometry, which gives spatial information about features and airway geometry much smaller than the imaging voxel size. The extraordinarily long T_1 of ^3He provides the opportunity to use stimulated echoes to probe long diffusion times and distances. Preliminary evidence indicates that for distances significantly larger than a pulmonary acinus (≥ 1 cm), the measured diffusivity is severely restricted (near 0.02 cm²/s) and is dominated by diffusion through collateral routes. This implies that the long-range *ADC* measurement of ^3He in lungs is an exquisitely sensitive measure of collateral airway paths.

1. Introduction

Our research group's focus is diffusion magnetic resonance imaging (MRI) of hyperpolarized ^3He gas in lungs. It is an application of the ideas of restricted diffusion applied to an unusual and especially high-value porous material, namely lungs. The goal is to learn as much as possible about the lung and its state of disease from MRI measurements of restricted diffusion.

Many people have expressed wonder that the phenomenon of nuclear magnetic resonance (NMR), a simple case of absorption by a two-level (or N-level) system, gave rise to the remarkable applications seen today. These include high resolution NMR to determine structures of organic and biological molecules in solution and in the solid-state and magnetic resonance imaging, to name just two. Similarly, we are impressed that the sensitivity of NMR to diffusion, first discussed by Hahn in his report of the discovery of spin echoes, would grow into the tool we see today [1]. For example, a large fraction of the papers at the previous Diffusion Fundamentals conference (and no doubt at this one) treat restricted diffusion measured by NMR or MRI. One currently exciting application is determining the direction of the fiber-axes in brain white matter tracts, allowing "the wiring bundles of the brain" to be visualized [2].

The basic idea of NMR measurement of diffusion uses a spin echo (or a gradient echo) with gradient-induced attenuation to detect displacements during the experiment. The spins precess in a spatially non-uniform field $B(x) = B_0 + Gx$, where G is the field gradient. After the first rf pulse (see top trace of Figure 1), a spin precesses and accumulates phase $\Phi_1 = \gamma G x_1 \tau$ just before the refocus (180°) pulse; x_1 is the time average position of the diffusing spin during this time. The field B_0 does not appear in this rotating-frame picture. The 180° pulse inverts the phase Φ_1 ; additional phase Φ_2 accumulates after the pulse. Using x_2 as the time average position after the second rf pulse, the total phase Φ is $\Phi = \Phi_2 - \Phi_1 = \gamma G \tau (x_2 - x_1)$.

Clearly the spin dephasing depends on (the distribution of) displacements $x_2 - x_1$. It is easy to complete this derivation for the case of free diffusion; there, the mean-squared displacement $\langle (x_2 - x_1)^2 \rangle = 2D_0\tau$. The correct result is only slightly more involved, $S(2\tau)/S(0) = \exp(-\gamma^2 G^2 D \tau^3 / 3) = \exp(-bD)$, where trivial relaxation terms are omitted and b is often used to represent $2\gamma^2 G^2 \tau^3 / 3$. This decay of echo amplitude S comes from the spread in spin phases Φ due to the distribution of displacements. The measured echo attenuation with varying G and/or τ allows D to be determined.

Using this simple constant-gradient technique, Woessner found systems in which the apparent diffusion coefficient (ADC , simply the value of D obtained from the above formula) was less than D_0 and depended on the diffusion time τ [3]. Thus, NMR was exploring restricted diffusion. An experimental verification of the physics in the equation above was performed by Stejskal and Tanner using time-dependent gradients and spin echoes [4].

A major technical improvement was the development of pulsed field gradients [3,4]. As in Figure 1, identical gradient pulses of width δ and separation Δ are used, allowing the spin signals to be detected and the rf pulses to be applied, all during periods of zero gradient. This allows much stronger gradients G to be used, to probe smaller values of ADC . If the pulses are comparatively narrow, $\delta \ll \Delta$, the diffusion-time is now well

defined and equal to Δ , sharpening the concept of time-dependent diffusion. In this case, $b = \gamma^2 G^2 \delta^2 \Delta$.

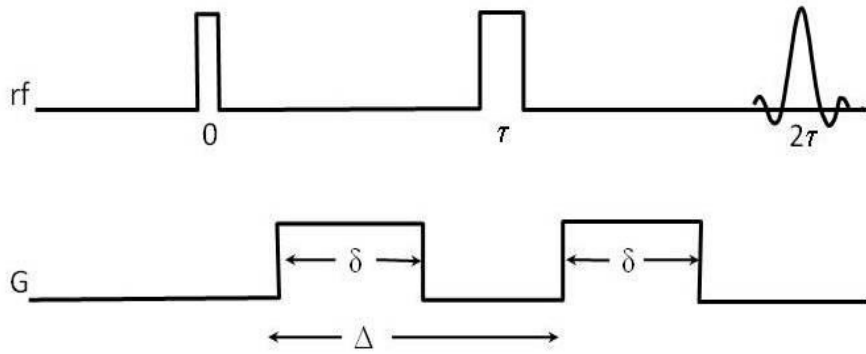


Fig 1: Timing of rf pulses and spin-echo, top trace. Lower trace shows field-gradient pulses.

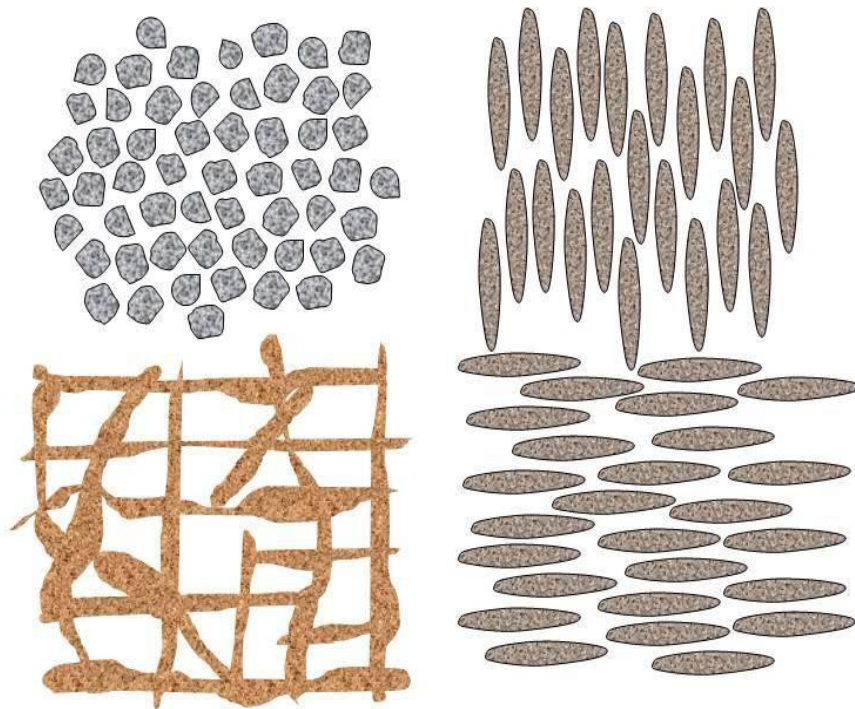


Fig 2: An atypical porous material, with regions of open (upper left) and closed (lower left) porosity. At right are anisotropic regions, showing locally preferred orientations of the pores. Shaded regions are material; unshaded regions are fluid.

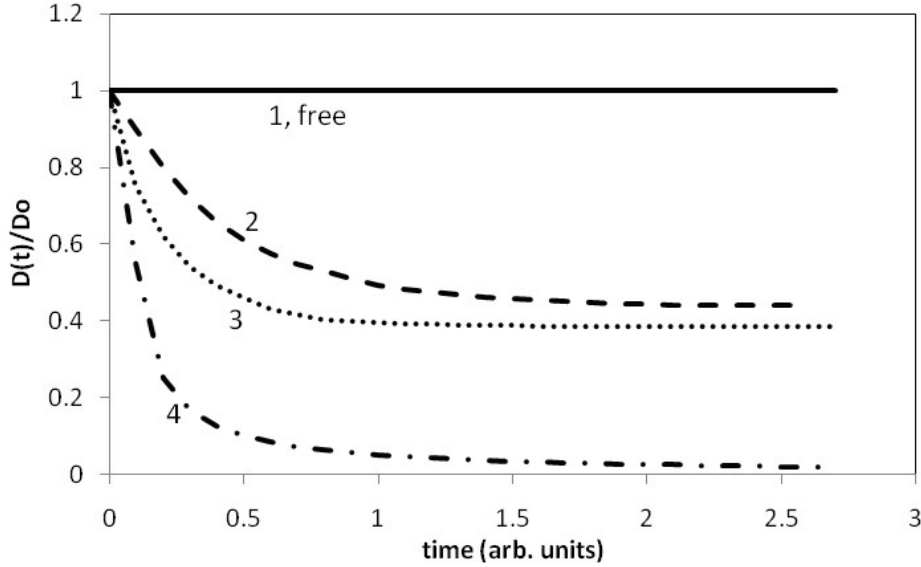


Fig 3: Sketch of ADC variation with diffusion time τ for four hypothetical porous systems. Curve 1 is for unrestricted diffusion, $ADC = D_0$. Curves 2 and 3 describe open porosity, so that the long-time limit of ADC is non-zero; the greater initial slope shows substance 3 to have a greater A/V than substance 2. Curve 4 describes a closed-pore system, so ADC approaches zero at long τ .

Consider the material sketched in Figure 2, where fluid fills the pores. Each region has a characteristic length L , typically the length between walls. In restricted diffusion, the crucial issue is the relative size of L (or in anisotropic regions, the several values of L) and the rms free displacement, $(2 D_0 \tau)^{1/2}$. Typical variations of ADC with diffusion time τ are given in Figure 3; normalized diffusivity ADC/D_0 is plotted there.

At very short diffusion times τ , the ADC approaches D_0 , because a vanishing fraction of the spins (or molecules) will experience the walls during the measurement. At somewhat longer times, but still in the limit $(2 D_0 \tau)^{1/2} < L$, only a small fraction of the diffusers will feel the wall during time τ . For this fraction, the diffusion is reduced while the remainder exhibit free diffusion. Thus, Mitra and Sen [5] derived their important result,

$$\frac{D(t)}{D_0} \approx 1 - \left(\frac{4}{9 \cdot \sqrt{\pi}}\right) \frac{A}{V} \cdot \sqrt{D_0 \tau} + o(D_0 \tau) \quad (1)$$

Thus, the slope of the decrease in ADC as a function of $\tau^{1/2}$ can provide the surface to volume ratio, A/V . We note that from dimensional considerations, A/V must be of order $1/L$.

At the other end of the scale, where $(D_0 \tau)^{1/2} < L$, the diffusing molecules thoroughly explore their environments (pores, walls, channels) in time τ . In typical porous systems,

this is the tortuosity limit; ADC/D_0 approaches the value $1/\alpha$, the tortuosity. In Fig. 3, α is clearly ∞ for curve 4, the closed pore system. Curves 2 and 3 share the same tortuosity (roughly 2), but have different A/V . To understand the tortuosity limit, think of school children running randomly through a forest. Each child has a unique story of bumping into trees, tripping over roots, wading through a stream, etc. Over a long enough time, however, each will have encountered the same statistical mixture of trees, roots, streams, and meadows; in this limit, each child's progress is slowed by a constant factor, the tortuosity. Bear treats this with more rigorous mathematics [6].

It will turn out (see below) that lung is not a typical porous material with a single characteristic length scale L . Instead, lung has hierarchical branching that cannot be described by a single L .

2. Hyperpolarized Gas

In order to obtain NMR/MRI signals with useful signal-to-noise ratio (S/N) from the low density of spins typical of gases, it is necessary to increase the spin *polarization* by laser-driven atomic-physics methods. On the one hand, such *hyperpolarization* can be regarded as a trivial technical detail in that it has no effect on the restricted diffusion behavior and serves only to increase S/N . On the other hand, almost none of the advances described herein would have been possible without the development of methods to generate large quantities of gas at high polarization.

The traditional way of obtaining spin polarization (i.e., more spins in one spin state than the other, for spins one-half) is to allow them to come to Boltzmann thermal equilibrium. At the practical level, this is easy—let the spins reside undisturbed in a strong field for a time longer than the relaxation time T_1 . Indeed 99+% of NMR/MRI uses this method. For water in humans, T_1 can be about 1 s. In a typical magnetic field used for MRI of 1.5 T, the energy difference between spin-up and spin-down of ^1H or ^3He nuclei is about 60 MHz (or equivalently 0.003 K). Clearly, at $T = 300$ K there will be nearly equal numbers of spins up and down. Using the high-temperature expansion of the Boltzmann factor yields

$$\frac{N_{\downarrow}}{N_{\uparrow}} = \exp\left(\frac{h \cdot f}{k \cdot T}\right) \approx 1 - \frac{h \cdot f}{k \cdot T} \quad (2)$$

where f is the NMR frequency and the nuclear spin polarization P is defined as

$$P \equiv \frac{N_{\uparrow} - N_{\downarrow}}{N_{\uparrow} + N_{\downarrow}} \approx \frac{h \cdot f}{2 \cdot k \cdot T} \quad (3)$$

For the numbers above, the equilibrium value of spin polarization P is about 5 ppm, meaning only this tiny fraction of spins are responsible for the detected NMR signals.

For biological tissue, which is mostly water, the density of hydrogen nuclear spins is high enough to deliver useful S/N , even at the low value of P calculated above. But for

gases, the combination of low spin-density and low P makes MRI at Boltzmann equilibrium very difficult.

^3He can be hyperpolarized, however, yielding large signals from this gas. There are two routes available, spin-exchange optical pumping (SEOP) through an alkali metal vapor and pumping on metastable helium atoms in the $2s$ state. Both work well; SEOP allows the use of gas at 1-20 bar pressures and can use readily available diode lasers. For the metastability route, suitable lasers are more expensive and the process is performed at mbar pressures, requiring a non-magnetic device to compress to useful pressures. SEOP works well on any inert gas with spin one-half nuclei (so ^3He and ^{129}Xe) while only ^3He can be pumped by the metastability approach. Both techniques transfer the angular momentum in photons of circularly polarized light to the nuclear spins. In the case of SEOP, the outer electrons of an alkali-metal vapor are polarized as an intermediate step.

Many research groups, including ours, use SEOP to polarize ^3He [7-9]. In the US, this is popular because MITI produced ~ 10 commercial SEOP polarizers; these are now part of GE Healthcare. There are numerous home-built polarizers, as well. A sample of 0.5-1.5 L STP is polarized in typically 12 h to 40% polarization, enough gas for perhaps 3 measurements on a live human subject. The 12 h time indicates that this process absolutely relies on the native- T_1 of the gas being quite long. Indeed, the intrinsic T_1 of ^3He at 10 bar is about 80 h; in appropriately cleaned glass vessels, T_1 is still 35-40 h, the decrease representing additional relaxation by interaction with spins in/on the walls.

Besides its spin one-half nucleus, ^3He has other important properties for diffusion-MRI. As mentioned above, its T_1 is long, allowing the gas to be hyperpolarized and delivered to the subject with most of its polarization remaining. Once exposed to the lung, T_1 decreases to only 15-20 s due to interaction with O_2 , which is paramagnetic (electron spin $S=1$) [10]. Thus ^3He MRI in-vivo is typically completed within 15 s of delivering the gas to the subject. The true transverse relaxation time T_2 is as long as T_1 . In lung, with its internal field gradient from the magnetic susceptibility difference between tissue walls and gas, the apparent T_2 is shorter. At 1.5 T, we find $T_2^* \sim 20$ ms in human lungs. This is still adequate time to acquire the spin signals in the MRI pulse sequences.

^3He has an extraordinarily large self-diffusion coefficient, D_0 . In ^3He at 1 bar, $D_0 = 2.4 \text{ cm}^2/\text{s}$, while dilute in air or N_2 at 1 bar, $D_0 = 0.88 \text{ cm}^2/\text{s}$ [8, 11]. These large diffusivities reflect the low mass and correspondingly high thermal velocity and reflect the small size of helium, giving it a long mean free path [12]. The large D_0 translates into ^3He exploring large distances in short times. The rms free displacement measured along one-dimension is $x_{\text{rms}} = (2 D_0 t)^{1/2}$, for diffusion time t . For $t = 2$ ms and ^3He diffusing in air or N_2 , x_{rms} is 600 μm . This is comparable to the mean acinar airway diameter (see below) of 700 μm . Thus, ^3He can explore distances relevant to lung features in a very short time, making ^3He diffusion – MRI an ideal probe of lung microstructure. Further, by using NMR methods that store magnetization parallel to the external field, the long time constant T_1 will permit even longer distance paths to be studied.

It is also possible to use Boltzmann-polarized gases for MRI in some circumstances [13]. Fluorinated gases like SF_6 , C_2F_6 and C_3F_8 are non-toxic and have many equivalent ^{19}F spins per molecule; their T_1 is convenient (1 – 20 ms) for rapid signal averaging, as described in more detail below. However, the signal-to-noise ratio S/N is generally inferior to hyperpolarized ^3He . There is a limited world-supply of ^3He (generated from

the decay of tritium used in thermonuclear weapons); this has driven some recent interest in hyperpolarized ^{129}Xe [14].

3. Lung as a Porous Medium

Since the noble gases discussed above have very large free diffusion coefficients (order $1\text{ cm}^2/\text{s}$) compared to liquids and relatively long transverse and longitudinal NMR relaxation times, these properties can be used to advantage in the study of media with large pores that are not easily studied with infused liquids. While a long T_1 is often viewed as a disadvantage in many MR applications because it causes longer recycle delays during signal averaging, here it allows measurement of diffusion of the molecules for times as long as T_1 . This corresponds to distances orders of magnitude larger than available via molecular gases with much shorter T_1 's (e.g., C_2F_6), and many orders of magnitude larger than one could achieve via liquids. In particular, restricted diffusion MR of hyperpolarized gases allows us to probe large-pore, low-surface-area, and complex media, such as lung. With free diffusivity $D_0 = 0.88\text{ cm}^2/\text{s}$, ^3He can diffuse an x_{rms} of almost 7 cm during its T_1 (in lung) of 25 s . In contrast, water has $D_0 \cong 2.5 \cdot 10^{-5}\text{ cm}^2/\text{s}$, so during a time equal to its T_1 of 1 second , x_{rms} is only $65\text{ }\mu\text{m}$ [2, 5].

Even though it is not traditionally viewed as simply a restricted medium, the lung is a particularly unique, challenging, and high-value medium to study. The high diffusivity D_0 of gas ensures the diffusion will be restricted by encounters with airway and alveolar walls, despite the low A/V (around $17\text{ m}^2/\text{L}$) and large "pore" size (around $300\text{ }\mu\text{m}$). By comparison, the diffusion of water, even at relatively long diffusion times, would be almost entirely unrestricted. The lung is indeed a particularly low surface-area substance when compared to activated charcoal (near $3000\text{ m}^2/\text{gram}$), the prototypical high A/V adsorbent.

Each living human, however, has at least one lung, which gives the medium an intrinsically high value. Moreover, lung disease is prevalent around the world, so understanding lung structure via noninvasive means is important to society. Singly-bifurcating airways extend from the trachea all the way to the smallest air sac, making lung structure and the interpretation of restricted diffusion different at different diffusion-length and diffusion-time scales. Further, the vast majority of the volume of gas spaces in lung demonstrate branching at lengths much smaller than typical imaging voxels, making single-airway imaging impossible. Since the gas diffusion and its interpretation are rather complicated and length-scale dependent in lung, it is important to detail lung structure in order to begin to understand the measurements of restricted diffusion.

Lung Structure

There are approximately 24 levels of airway branching in human lung, from generation $Z = 0$ (trachea) to generation $Z = 23$ (terminal alveolar sacs), as depicted in Figure 4 [15]. Human lung branches in such a way that facilitates effective gas flow

(convective, or hydrodynamic) from $Z = 0$ to $Z = 13$ and effective diffusive gas transport from $Z = 14$ to the terminus, for normal inspiratory pressures less than 25 cm H₂O. The lung is thus often divided into two regions: the “conducting” zone and the “respiratory” (diffusive transport) zone. Throughout the respiratory zone, oxygen and carbon dioxide can dissolve through thin airway or alveolar walls and exchange into or out of blood. Each region supplied by a terminal bronchiole (nominally $Z=13$) airway is called an acinus. Conductive airways’ diameters follow an inverse power law, $d(Z) = d_0 2^{-Z/3}$, with increased numbers of branches at each generation ($N(Z) = 2^Z$) to maintain efficient flow. Acinar airways ($Z > 13$), by contrast, maintain a near-constant diameter from $Z = 14$ to $Z = 23$, with increasing numbers of alveoli lining the airway with increasing generation number (Figures 4 and 5). On average, the major radius of the acinar airways in healthy human lung is around 350 microns [15].

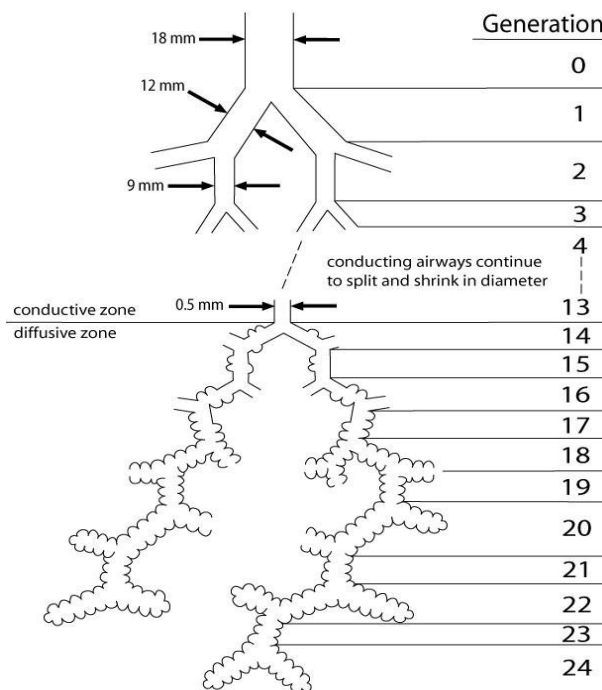


Fig 4: Human lung structure [15]. The “diffusive” zone (levels 13-24) comprises around 94% of the total volume of the lung, implying an imaging voxel is representative largely of levels 13-24 (the acinar airways).

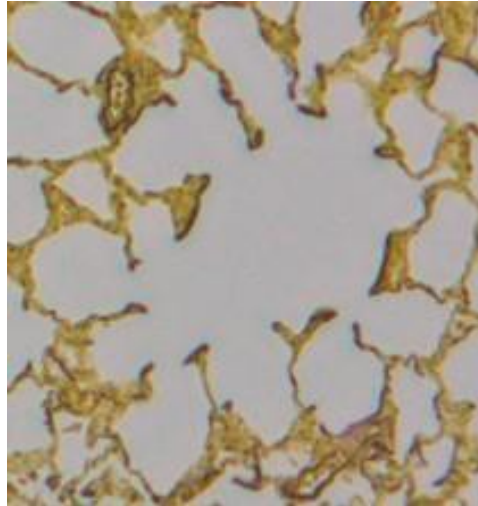


Fig 5: Example of an acinar airway in a dog lung (long axis perpendicular to the page), with alveoli lining the nominally cylindrical geometry. This represents one airway at branching levels 15-24 in Figure 4. A geometrical model is presented in Figure 6.

Diffusion within a bifurcating structure leads to very unique properties that depend critically on the measurement details, such as timescale or length scale of the measurement. In effect, this is diffusion within a complicated fractal network of branching airways. While there is some early research in random walks in organized and random networks (e.g., information diffusion through social networks on the worldwide web), there is no theoretical framework through which restricted diffusion in lung can be modeled for all length scales [16, 17]. In contrast to the excellent work in the fields of rocks and bead packs [16, 18-20], the work in restricted diffusion in lung has been led largely by explorations at single time scales and length scales up to this point.

One can think of this type of diffusion in analogy to a random walker exploring a singly-connected set of hiking trails, where there is only one route between any two points on the mountainside. During the shortest times (less than a second) the walker can't reach the edge of the path, so unrestricted diffusion is measured. At very short times of a few seconds, the random walker explores only the boundaries of the current section of the path (sampling effectively the boundary-to-area ratio). During times of a few minutes, the walker has time to explore some of the length of the current path, with high probability of staying between branching points (sampling both the width of the path and the ease of traveling up or down the path). At very long times (many hours or days), it's likely that the walker will travel between many branch points; in this case the probability of traveling between any two specific points far away is very low and depends critically on the amount of time passed. In this analogy there is no "tortuosity limit" which would

characterize the interconnectedness of the mountain-path network. That is to say, there is no asymptotic long-time limit of connectivity that characterizes the difficulty of traveling between two arbitrary points on the network in this singly-connected scheme. Of course the existence of “shortcuts”, or routes beyond the singly-connected hiking trails, changes everything and may allow a tortuosity limit. As we will see, these shortcut (collateral) paths are very important in long-distance diffusion in lung.

4. Imaging Lung Microstructure via Diffusion

Before we attempt an in-depth exploration of imaging gas diffusion in lung, it is important to answer the question of why one should perform imaging instead of whole-sample measurements. After all, to obtain useful S/N from each small voxel is much more difficult than measurements from, say, an entire lung filled with gas. This lower S/N in imaging then requires use of hyperpolarized gas. There are several answers to this question. First and foremost, human lung disease is often heterogeneous; thus, spatially resolved measurements are important in understanding the nature, pathogenesis, and progression of disease. Further, for a small region with structure altered by disease, a non-selective bulk measurement can easily obscure the changes in the small region. Spatial resolution also allows the comparison of structure with the lung’s ventilation (air pumping) function: the number of gas atoms within an imaging voxel is directly relevant to the obstruction of conducting airways leading to the voxel. This spatially-resolved ventilation can be compared with the average regional alveolar structure to form better structure-function relationships [21].

Since lung airways are singly connected and bifurcating, in order to effectively image the structure of this unique medium, one must experimentally explore restricted diffusion at a broad range of timescales. Stated differently, we must explore the $D(t)/D_0$ curve (Figure 3) for all relevant scales to understand lung structure and connectivity. Clearly, measuring at short-enough times can lead one to approach the surface-to-volume limit, and at long-enough timescales the diffusivity will approach zero for true, singly-connected pathways. Establishing and connecting these two limits has been the subject of lung diffusion MR research over the last few years.

Short times

The Taylor expansion from Eq. 1 in powers of $(D_0 t)^{1/2}$ is valid when only a small fraction of molecules encounter boundaries, or when $A/V (D_0 t)^{1/2} \leq 1$. The short time limit is achieved when a typical random walker has only a small probability of colliding with a boundary. Thus, by measuring the linear decrease of $D(t)/D_0$ as a function of $(D_0 t)^{1/2}$, one can measure the surface to volume ratio, A/V [5, 22, 23]. Standard clinical MR imagers (which can accommodate a human volunteer or an entire human lung) typically allow diffusion times of 1-2 ms at a minimum due to finite time requirements (limited slew rates) for the required field gradients. The large diffusion coefficient of ^3He , at $0.88 \text{ cm}^2/\text{s}$ dilute in air, results in $A/V (D_0 t)^{1/2}$ of around 10.5 for a diffusion time of 2 ms and typical

human-lung A/V of 250 cm^{-1} [24], putting it well outside the short-time limit. To reduce this number to unity, the diffusion time would need to be 100 times smaller, or about $20 \mu\text{s}$, which is much shorter than current or foreseeable gradient technology would allow (20 mT/m , at a slew rate of 120 T/m/s , is a typical value). ^{129}Xe , with a much lower free diffusion coefficient of $0.057 \text{ cm}^2/\text{s}$, would get closer $A/V (D_0 t)^{1/2} = 2.7$, for a 2 ms diffusion time in healthy lung). For the case of dilute xenon in air, the diffusivity is increased, pushing it even further away from the A/V limit [25].

By contrast, the stable perfluorinated gases (SF_6 , C_2F_6 , etc.), while not hyperpolarizable, have free diffusion coefficients near $0.03 \text{ cm}^2/\text{s}$, putting them closer to the surface-to-volume limit for MR-determined restricted diffusion [26, 27]. They also have very short T_1 's and have been used for some imaging applications by rapid signal averaging [28-30]. An early successful method of collecting gas MR signals in rat lung and calculating regional ventilation and perfusion was demonstrated by Keuthe, *et al.* [13, 26]. He collected FID data very quickly using radial scanning of k-space with essentially static field gradients, for measurements of gas concentration (and thus ventilation/perfusion ratios, since the T_1 is dependent on oxygen concentration). Later, Ruiz-Cabello *et al.* used SF_6 to measure restricted diffusion in small animals via projection reconstruction [31]. More recently, researchers have quantified ventilation and ventilation-perfusion ratios in animals by using fast gradient echoes and FID-projections, respectively [32, 33].

Jacob *et al.* capitalized on the longer relaxation times of stable fluorocarbons (C_2F_6 , C_3F_8) to perform MR diffusion imaging with explanted human lungs in a clinical scanner [30]. They demonstrated significant diffusion restriction (x2) with reasonable signal to noise (near 10). Sufficient contrast was achieved to clearly distinguish normal tissue from larger alveoli characteristic of emphysema, with a factor of 2 change in apparent diffusion coefficient. This represented a step forward in the utility of perfluorinated gas imaging as a surrogate for lung morphometry, and while this represented relatively short diffusion times, the true short-time limit has yet to be achieved by these gases [34].

One recent, encouraging development came from the Virginia group in the short-time regime for ^3He [35]. By concatenating a large number of bipolar gradient pulses and sampling between neighboring pulse pairs, they were able to increase the diffusion attenuation while maintaining a very short effective diffusion time. They achieved experimental diffusion times ranging from 200 to $700 \mu\text{s}$ with this method—well below what can be measured using the conventional method. While not yet extended to measurements in human lung, simulations and proof-of-principle experiments in spherical containers bode well for the probability of accurate A/V measurements in the lung with ^3He .

Medium Times

Most hyperpolarized gas diffusion MR imaging has been performed in what we call here the medium-time regime [9, 11, 36]. In lung this is when gas atoms almost certainly collide with the airway wall one or more times, but have little probability of leaving the acinar airway in which they started. For ^3He this corresponds to times of a few

milliseconds. Multiple gas-tissue interfaces (alveoli) in the lung complicate the measurements, however. The resulting T_2^* is relatively short (20 ms), which limits the range of diffusion times that can be used. (Almost all hyperpolarized MRI uses gradient echoes to avoid the large rf pulses of spin echoes, in order to preserve most of the magnetization for later use.) T_2^* can be lengthened by imaging at lower field strength [14, 37].

Chen et al. were the first to demonstrate significantly restricted ^3He diffusion in the lungs of healthy guinea pigs, with a ^3He ADC near $0.16 \text{ cm}^2/\text{s}$ and a non-dilute free value of $2.4 \text{ cm}^2/\text{s}$ at a diffusion time of around 1 ms [8]. (We measure a non-dilute free value near $1.9 \text{ cm}^2/\text{s}$ in our lab.) The first evidence of the simple technique's ability to distinguish healthy from enlarged alveoli, however, came from Saam *et al.*, in 2000 [11]. There, truly high-contrast between the apparent diffusion coefficient in healthy ($0.2 \text{ cm}^2/\text{s}$) and emphysematous lungs ($0.5 - 0.6 \text{ cm}^2/\text{s}$) was shown, giving rise to the possibility that the technique could be used to quantitatively characterize the extent and spatial location of alveolar enlargement, which was previously possible only with a physical lung sample under the microscope. The result of ADC near $0.2 \text{ cm}^2/\text{s}$ in healthy human lung for diffusion times of $1.5 - 3 \text{ ms}$ was also confirmed by many other research groups [9, 36, 37, 39-42].

A significant increase in understanding came when the restricted diffusion was linked with a realistic model of acinar airways by Yablonskiy *et al.* in 2002, based on the known geometrical structure of the lung, reported by Weibel [15, 43]. In this model diffusion anisotropy is predicted within each acinar airway, with greater diffusion parallel to the airway axis than transverse. Despite the microscopic anisotropy, each imaging voxel contains hundreds of such airways with essentially all orientations, making each voxel have macroscopically isotropic diffusion properties. Thus, the microscopic anisotropy (of each airway) is only manifested in the MR signal as a non-exponential decay. That is, the decay of signal as a function of b -values is fastest for airways parallel to the diffusion sensitizing gradient, while the signal decay is slowest for airways transverse to the gradient. Summing over all airway orientations, a non-exponential signal decay results from this microscopic diffusion anisotropy. Under a diffusion tensor formalism with principal values D_L (longitudinal) and D_T (transverse), a closed-form solution was derived:

$$S = S_0 \cdot \exp(-b D_T) \cdot \sqrt{\frac{\pi}{4b(D_L - D_T)}} \cdot \text{erf}(b(D_L - D_T)) \quad (4)$$

D_T is then related to the major airway radius R (Figure 6) via a Bessel function [43]. The first *in-vivo* results for major-airway radius (0.35 mm) in healthy volunteers matched *ex-vivo* morphometric studies to within a few percent—an early success of this model. Since separation of the anisotropic components of the restricted diffusivity allowed an *in-vivo* morphometric measurement, it was proposed that this method can serve as a new gold standard for airspace size, previously available only under the microscope with excised tissue. The theoretical framework was recently improved, with calculated accuracy ranges on the equations' ability to accurately model acinar airways of differing

radii [44]. Importantly, the alveolar “sleeves” that cover acinar airways are given an idealized but physiologically accurate structure, as in Figure 6. The improvements yield small corrections to the dependence of D_T to the radius R and allow D_L to serve as a measure of the ratio r/R (r is the minor radius, as in Figure 6). An underlying assumption remains that the cylindrical airways are long enough that leakage of spins from one airway to the next is negligible during the diffusion measurement (For these measurements, Δ is 1.8 ms and the total gradient waveform duration is 3.6 ms.). We are exploring this limitation now by computer diffusion simulations. A phenomenological interpretation of multi-component diffusion was offered by Trampel *et al.* in terms of diffusional kurtosis, but without the accompanying relation to alveolar geometry [45, 46]. Jacob *et al.* confirmed that the model in Eq. (4) provides excellent signal description in a very broad range of b -values, while the kurtosis model does not [46].

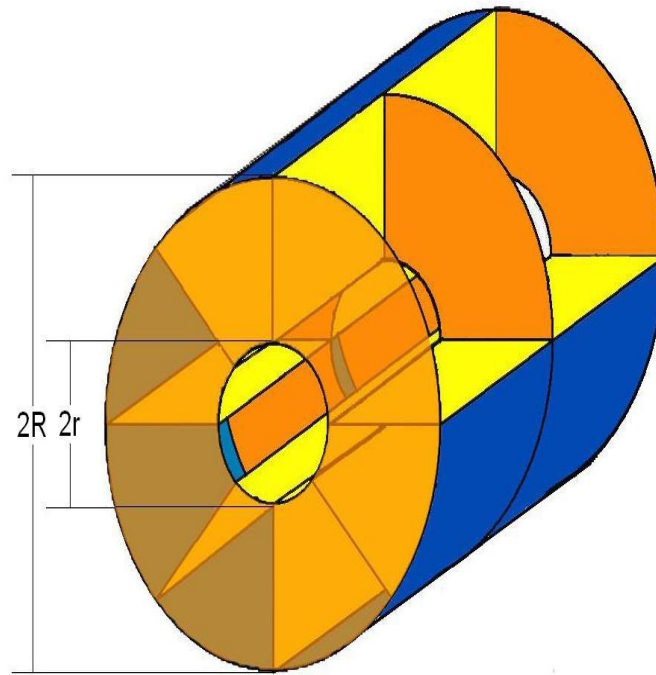


Fig 6: Detail of an acinar airway from the cylindrical model of airways in the human pulmonary acinus. The ratio of minor to major radii r/R is related to D_L and the major radius R is related to D_T .

Long times

The first evidence of starkly different long-time behavior (diffusion times of several seconds) of ^3He diffusion in lung was by an MR group at the University of Nottingham . They capitalized on the long T_1 of ^3He by storing the diffusion-sensitized spin magnetization along the z -axis in a stimulated echo. Owers-Bradley, et al. measured long-time stimulated echoes *in vivo* in humans and found an apparent diffusion coefficient near $0.02 \text{ cm}^2/\text{s}$ [47]. Their experiment demonstrated monoexponential decay of the ^3He stimulated echo, implying that the ADC is time-independent over the (narrow) range of 1 - 5 seconds. They tagged longitudinal magnetization in lung and plotted a linear relationship between the rate of tag decay and k^2 (equal to $4\pi^2/\lambda^2$), also implying no length dependence of the ADC . The lack of apparent length dependence was puzzling, since the ADC at 2 ms times is clearly much larger ($0.2 \text{ cm}^2/\text{s}$), implying some diffusion-length dependence [9, 11, 48]. The answer lies in the range of tagging wavelengths studied (1-4 cm), which represents distances *much* longer than the diffusion distances measured previously with 2-ms diffusion times. That is, the length dependence (or time dependence) is a slowly varying function. Perhaps more importantly, 1 cm is slightly larger than the size of the human pulmonary acinus, within which diffusion is relatively effective at gas transport (by design) and outside of which diffusion is much less effective.

Subsequently, Woods, *et al.* used a similar technique to measure the long-distance diffusion in canine lungs [49]. Sinusoidally modulated longitudinal magnetization with wavelength λ was prepared by two 45-degree rf pulses separated by a gradient pulse of duration t and magnitude G such that $\gamma G \lambda t = 2\pi$ (The use of 45-degree rf pulses avoids rectified negative magnetization that would appear in magnitude images that are standard with gradient echo imaging sequences.). By spatially modulating the longitudinal magnetization and then monitoring the sinusoidal contrast over long times, it is possible to separate the effects of T_1 and rf magnetization consumption, as opposed to gas diffusion. One begins with initial magnetization $M = M_0 (1 - \sin(kx))$, as results from the pair of 45° pulses. Homogenization of the sinusoid is governed by the diffusion equation $\partial M / \partial t = D' \Delta M$, the relevant solution for 45° pulses is

$$M(x, t) = 1/2 \cdot M_0 \cdot [1 - \sin(kx) \cdot \exp(-Rt)], \quad (5)$$

where M_0 and R are respectively the initial magnetization and the rate of decay due to diffusion only, without relaxation. The apparent diffusivity D' is related to the decay rate R of the spatial modulation by $R = D' k^2$. The operative solution including relaxation is thus

$$M(x, t) = \frac{1}{2} M_0 \cdot \exp(-\frac{t}{T_1}) [1 - \sin(kx) \cdot \exp(D' k^2 t)], \quad (6)$$

for full modulation depth. Two advantages to long-range diffusion imaging, as opposed to spectroscopy, are that the amount of restricted diffusion can be spatially localized to

within approximately one tagging wavelength and that diffusion is probed at a specified length scale.

Using this technique Woods *et al.* measured $0.02 \text{ cm}^2/\text{s}$ in the canine lung for tagging wavelengths (approximate diffusion distance) of both 2 and 3 cm [49, 50]. Lungs with spatially varying degrees of elastase-induced emphysema were studied, and $D_{2\text{-cm}}^*$ as high as $0.2 \text{ cm}^2/\text{s}$ was observed in certain regions [49]. This prompted a similar study in human lungs, both healthy and with emphysema. Results in these explanted human lungs with normal alveolar structure were consistent with previous studies, with diffusion coefficients at $0.02 \text{ cm}^2/\text{s}$ for 2-cm tagging wavelengths [50]. Maps of the long-distance diffusion in healthy and emphysematous lungs were then compared to measurements of alveolar integrity by observation of tissue under the microscope, with reasonable correlation. This demonstrated that such long-range diffusion is sensitive to the *effective* tortuosity of the medium. That is, there is greater connectivity in regions with emphysematous tissue loss and increased inter-acinar openings, resulting in enhanced long-range gas diffusion.

More recently, Wang *et al.* demonstrated diffusion measurements at multiple diffusion times during a single breath hold [51]. For a tagging wavelength of 1 cm, the Virginia group reported measurements that ranged from $0.05 \text{ cm}^2/\text{s}$ to $0.01 \text{ cm}^2/\text{s}$ for times 0.5 s to 9 s, respectively. This emphasizes that both the experimental length-scale (here, a tagging wavelength of 1 cm) and the timescale are critically important, even though the time and length scale are linked (longer experiment times implies longer diffusion length).

We interpret this time and length dependence in light of the complicated structure of human lung described in section 3 above. Since airways within the pulmonary acinus are particularly effective at diffusive transport of O_2 to alveolar surfaces (through which it diffuses across the tissue to blood), we expect that ADC on timescales and length-scales relevant to diffusion within the acinar airways will be significantly different from longer-scale, interacinar diffusion. During times of a few milliseconds and lengths shorter than 1 mm (as reported in Medium Times above), the diffusivity in normal lungs is near $0.2 \text{ cm}^2/\text{s}$ and reflective of individual acinar-airway geometry. At long times and length-scales [47, 49-51], atoms must diffuse out of the acinus (along the airways or via a collateral route) to effect tagging decay. The measured diffusion is concomitantly low, at or near $0.02 \text{ cm}^2/\text{s}$, since inter-acinar gas movement is expected to be very slow via diffusion. During the intermediate times of less than a second and length-scales *near* the size of the acinus (around 0.6 cm in length), we expect for there to be non-uniform decay, with short-time ADC values (sensitive to diffusion throughout the acinus) higher than long-time ADC values (involving inter-acinar diffusion).

This is indeed what was seen in the computer simulation work of Bartel *et al.*: magnetization will only decay a limited amount from intra-acinar motions alone [52]. This was demonstrated for 2-cm wavelengths; only 20-25% of the magnetization modulation will decay from intra-acinar diffusion, leaving the bulk of the measurement reporting inter-acinar or collateral diffusion. Recent work on intra-acinar diffusion was performed by Verbanck and Paiva and confirmed this, with a simulated result of $0.02 \text{ cm}^2/\text{s}$ for diffusion throughout an individual acinus [53]. Our group's simulations in singly-bifurcating lungs with no collateral connections showed extremely low

(interacinar) ^3He diffusivity— $D' = 0.0009 \text{ cm}^2/\text{s}$ for 2-cm tagging wavelengths. This was much lower than has been measured experimentally, implying that the experimentally measured value may be particularly sensitive to collateral connections in lung. Experiments in a porcine lung, known to have fully septated lobules (impenetrable to ^3He atoms) and thus much lower collateral connectivity, demonstrated much lower diffusivity ($0.004 \text{ cm}^2/\text{s}$), supporting this claim. Therefore, the measurements near $0.02 \text{ cm}^2/\text{s}$ for long-range ^3He ADC in healthy human lung appear to reflect the number and extent of collateral pathways.

Conclusion

Restricted diffusion of gas in the lung is in many ways similar to restricted diffusion in other porous media: atomic collisions with boundaries restrict the measured value, and there is a critical dependence on the time and distance scales of the measurement. Gases provide a much larger free diffusion coefficient than liquids, allowing large pores (350 microns, the size of a human alveolus) to be studied. Hyperpolarization permits imaging diffusion of the gas itself, despite the 1000 times lower spin density compared to liquids. Fluorinated hydrocarbons don't deliver the high signal to noise available with hyperpolarized ^3He but are easier to use and are a future alternative. The complicated nature of bifurcating human lung structure provides challenges in interpretation of results. At times sufficiently short such that $A/V (D_0 t)^{1/2} \leq 1$, the short-time slope of $D(t)/D_0$ (as a function of the square root of diffusion time) is proportional to A/V , an important measure of lung structure and early emphysema. However, this short-time limit has not yet been obtained in lungs. During times of a few milliseconds, diffusion anisotropy is observed, and the principal components of diffusion are related to geometric parameters of individual acinar airways. This permits regional *in-vivo* lung morphometry, which gives spatial information about features and airway geometry much smaller than the imaging voxel size. The extraordinarily long T_1 of ^3He provides the opportunity to use stimulated echoes and probe long diffusion times and distances. Preliminary evidence indicates that for distances longer than 1 cm (significantly longer than a pulmonary acinus), the measured diffusivity is dominated by diffusion through collateral routes. This implies that a long-time asymptotic limit may be observed in human lung for diffusion distances of a few centimeters, whereas no such limit would be obtained in the absence of collateral pathways.

References

- [1] Hahn, E.L., Physical Review, 1950. 80: p. 580-594.
- [2] Schaefer, P.W., P.E. Grant, and R.G. Gonzalez, Radiology, 2000. 217(2): p. 331-45.
- [3] Woessner, D.E., J Phys Chem, 1963. 67: p. 1365-1367.
- [4] Stejskal E.O. and Tanner J.E., J Chem Phys 1965. 42: p. 288-292.
- [5] Mitra, P.P., P.N. Sen, and L.M. Schwartz, Phys Rev B Condens Matter, 1993. 47(14): p. 8565-8574.
- [6] Bear, J., Dynamics of fluids in porous media. 1972, New York: American Elsevier.
- [7] LeaWoods J.C., et al., Concepts in Magnetic Resonance, 2001. 13: p. 277-293.

- [8] Chen, X.J., et al., *Magn Reson Med*, 1999. 42(4): p. 721-8.
- [9] Salerno, M., et al., *Radiology*, 2002. 222(1): p. 252-60.
- [10] Saam, B., W. Happer, and H. Middleton, *Phys Rev A*, 1995. 52(1): p. 862-865.
- [11] Saam, B.T., et al., *Magn Reson Med*, 2000. 44(2): p. 174-9.
- [12] Reif, F., *Fundamentals of Statistical and Thermal Physics*. 2008, New York: McGraw-Hill.
- [13] Kuethe, D.O., et al., *Magn Reson Med*, 1998. 39(1): p. 85-8.
- [14] Patz, S., et al., *Acad Radiol*, 2008. 15(6): p. 713-27.
- [15] Haefeli-Bleuer, B. and E.R. Weibel, *Anat Rec*, 1988. 220(4): p. 401-14.
- [16] Latour L. L. , Mitra P.P., Kleinberg R. L., and Sotak C. H., *J Magn Reson*, 1993. 101: p. 342-346.
- [17] Gallos, L.K., C. Song, and H.A. Makse, *Phys Rev Lett*, 2008. 100(24): p. 248701.
- [18] Hurlimann, M.D., L.L. Latour, and C.H. Sotak, *Magn Reson Imaging*, 1994. 12(2): p. 325-7.
- [19] Cory, D.G. and A.N. Garroway, *Magn Reson Med*, 1990. 14(3): p. 435-44.
- [20] Song, Y.Q., S. Ryu, and P.N. Sen, *Nature*, 2000. 406(6792): p. 178-81.
- [21] Fain, S.B., et al., *Acad Radiol*, 2008. 15(6): p. 753-62.
- [22] Mair, R.W., et al., *Phys Rev Lett*, 1999. 83(16): p. 3324-7.
- [23] Mair, R.W., et al., *J Magn Reson*, 2002. 156(2): p. 202-12.
- [24] Coxson, H.O., et al., *Am J Respir Crit Care Med*, 1999. 159(3): p. 851-6.
- [25] Mair, R.W., et al., *J Magn Reson*, 1998. 135(2): p. 478-86.
- [26] Kuethe, D.O., et al., *J Appl Physiol*, 2000. 88(6): p. 2279-86.
- [27] Schreiber, W.G., et al., *Magn Reson Med*, 2001. 45(4): p. 605-13.
- [28] Beyea, S.D., et al., *Magn Reson Imaging*, 2003. 21(3-4): p. 201-5.
- [29] Lizak M. , Conradi M.S., *J Magn Reson*, 1991. 95: p. 548-557.
- [30] Jacob, R.E., et al., *Magn Reson Med*, 2005. 54(3): p. 577-85.
- [31] Ruiz-Cabello, J., et al., *Respir Physiol Neurobiol*, 2005. 148(1-2): p. 43-56.
- [32] Scholz, A.W., et al., *Magn Reson Imaging*, 2009. 27(4): p. 549-56.
- [33] Adolphs, N.L. and D.O. Kuethe, *Magn Reson Med*, 2008. 59(4): p. 739-46.
- [34] Conradi, M.S., et al., *J Magn Reson*, 2004. 169(2): p. 196-202.
- [35] Carl, M., et al., *J Magn Reson*, 2007. 189(2): p. 228-40.
- [36] Moller, H.E., et al., *Magn Reson Med*, 2002. 47(6): p. 1029-51.
- [37] Durand, E., et al., *Magn Reson Med*, 2002. 47(1): p. 75-81.
- [38] Chen, X.J., et al., *Magn Reson Med*, 1999. 42(4): p. 729-37.
- [39] Fain, S.B., et al., *Radiology*, 2006. 239(3): p. 875-83.
- [40] Morbach, A.E., et al., *J Magn Reson Imaging*, 2005. 21(6): p. 765-74.
- [41] Swift, A.J., et al., *Eur J Radiol*, 2005. 54(3): p. 352-8.
- [42] Altes, T.A., et al., *J Magn Reson Imaging*, 2006. 24(6): p. 1277-83.
- [43] Yablonskiy, D.A., et al., *Proc Natl Acad Sci U S A*, 2002. 99(5): p. 3111-6.
- [44] Sukstanskii, A.L. and D.A. Yablonskiy, *J Magn Reson*, 2008. 190(2): p. 200-10.
- [45] Trampel, R., et al., *Magn Reson Med*, 2006. 56(4): p. 733-7.
- [46] Jacob, R.E., G. Laicher, and K.R. Minard, *J Magn Reson*, 2007. 188(2): p. 357-66.
- [47] Owers-Bradley, J.R., et al.; *J Magn Reson Imaging* 2002. 17(1): p. 142-146.
- [48] Peces-Barba, G., et al., *Eur Respir J*, 2003. 22(1): p. 14-9.
- [49] Woods, J.C., et al., *Magn Reson Med*, 2004. 51(5): p. 1002-8.

- [50] Woods, J.C., et al., *J Appl Physiol*, 2005. 99(5): p. 1992-7.
- [51] Wang, C., et al., *Magn Reson Med*, 2006. 56(2): p. 296-309.
- [52] Bartel, S.E., et al., *J Appl Physiol*, 2008. 104(5): p. 1495-503.
- [53] Verbanck, S. and M. Paiva, *J Appl Physiol*, 2007. 103(1): p. 249-54.